


BRIEF COMMUNICATION

High-resolution MRI of the human palatine tonsil and its schematic anatomic 3D reconstruction

Karl-Heinz Herrmann¹ | Franziska Hoffmann² | Günther Ernst³ | David Pertzborn² | Daniela Pelzel² | Katharina Geißler³ | Orlando Guntinas-Lichius³ | Jürgen R. Reichenbach^{1,4} | Ferdinand von Eggeling^{4,5} 

¹Medical Physics Group, Institute for Diagnostic and Interventional Radiology, Jena University Hospital, Jena, Germany

²Department of Otorhinolaryngology, MALDI Imaging and Innovative Biophotonics, Jena University Hospital, Jena, Germany

³Department of Otorhinolaryngology, Head and Neck Surgery, Jena University Hospital, Jena, Germany

⁴Michael-Stifel-Center for Data-Driven and Simulation Science Jena, Jena, Germany

⁵Department of Otorhinolaryngology, MALDI Imaging and Core Unit Proteome Analysis, DFG Core Unit Jena Biophotonics and Imaging Laboratory (JBIL), Jena University Hospital, Jena, Germany

Correspondence

Ferdinand von Eggeling,
Universitätsklinikum Jena, Am Klinikum 1,
07747 Jena, Germany.
Email: feggeling@med.uni-jena.de

Abstract

The palatine tonsils form an important part of the human immune system. Together with the other lymphoid tonsils of Waldeyer's tonsillar ring, they act as the first line of defense against ingested or inhaled pathogens. Although histologically stained sections of the palatine tonsil are widely available, they represent the tissue only in two dimensions and do not provide reference to three-dimensional space. Such a representation of a tonsillar specimen based on imaging data as a 3D anatomical reconstruction is lacking both in scientific publications and especially in textbooks. As a first step in this direction, the objective of the present work was to image a resected tonsil specimen with high spatial resolution in a 9.4 T small-bore pre-clinical MRI and to combine these data with data from the completely sectioned and H&E stained same palatine tonsil. Based on the information from both image modalities, a 3D anatomical sketch was drawn by a scientific graphic artist. In perspective, such studies could help to overcome the difficulty of capturing the spatial extent and arrangement of anatomical structures from 2D images and to establish a link between three-dimensional anatomical preparations and two-dimensional sections or illustrations, as they have been found so far in common textbooks and anatomical atlases.

KEYWORDS

3D reconstruction, 9.4 T MRI, anatomical reconstruction, histology, palatine tonsil

1 | INTRODUCTION

The tonsils are part of the body's immune defenses and are the first line of guard against inhaled or swallowed substances. As such, they serve as protection against pathogens that enter through the nasopharynx or oropharynx. They include the palatine tonsil, the lingual tonsil, the

pharyngeal tonsil, and the tubal tonsil or lateral cord. While palatine and tubal tonsils are present in pairs, the lingual and pharyngeal tonsils are unpaired. All together form the lymphatic pharyngeal ring (Waldeyer's pharyngeal ring). The palatine tonsil, for example, shows a specific functional compartment system consisting of the lymphoid follicles, parafollicular areas and the crypt epithelium (Nave et al., 2001).

Karl-Heinz Herrmann and Franziska Hoffmann are contributed equally as first authors.

Jürgen R. Reichenbach and Ferdinand von Eggeling are contributed equally as senior authors.

This is an open access article under the terms of the Creative Commons Attribution-NonCommercial License, which permits use, distribution and reproduction in any medium, provided the original work is properly cited and is not used for commercial purposes.

© 2021 The Authors. *Journal of Anatomy* published by John Wiley & Sons Ltd on behalf of Anatomical Society.

Although histologically stained sections of the palatine tonsil are widely available, they represent normal or pathologic tissue in two-dimensions only, lacking reference to three-dimensional space. However, tomographic imaging techniques suitable for 3D imaging and routinely used in clinical applications, such as PET/CT or MRI, are unable to provide the required spatial resolution. Optical techniques, such as optical coherence tomography (OCT) (Krafft et al., 2018), have very good spatial resolution but are limited in terms of penetration depth and applicability to excised samples. Attempts have been made to distinguish inflamed from non-inflamed palatine tonsils using Fourier transform infrared imaging (FTIR) (Piqueras et al., 2015), but analysis of the huge data sets is quite extensive and requires sophisticated complex analysis protocols.

The aim of our study was to take a first step toward high spatial resolution 3D imaging of a human palatine tonsil using pre-clinical high-field MRI on a resected tonsil specimen and to combine these data with the data from the fully sectioned and H&E-stained same palatine tonsil. Based on the information from both imaging modalities, a 3D anatomical sketch was created by a scientific graphic artist, which to our knowledge is the first of its kind.

2 | METHODS

2.1 | Human tonsil tissue sample preparation

The specimen was a right human tonsil resected from a 2-year-old male patient with tonsil hyperplasia. The procedure was in accordance with the ethical standards of the Jena University Hospital (vote of the ethics committee 3972-01/14 and 2019-1307) and the Helsinki Declaration from 1975 and its revision in 1983. Parents of the patient gave their written informed consent.

Immediately after tonsillectomy, the specimen was placed in a 4% formalin solution, fixed for 12 h, and carefully placed into a 15 ml PP cellstar tube (Greiner bio-one, 72636). To avoid movement during the long MRI scan times, granulated superabsorbent (HVDE 313, ElaDe.de, 74348) was added to thicken the formalin solution. The scans were performed after >24 h fixation time.

2.2 | MRI imaging

Scanning was performed with a 9.4 T small-animal MRI scanner using a 23 mm quadrature volume resonator (Bruker Biospin). The imaging protocol included the following sequences, each with 100 μ m isotropic resolution:

1. A 3D multi-echo gradient-echo (MEGE) sequence with matrix size $280 \times 160 \times 160$ and field-of-view, FoV = $(28 \times 16 \times 16)$ mm³. Twenty gradient echoes were acquired equidistantly ($TE_1 = 1.62$ ms, $TE_{20} = 43.9$ ms, $\Delta TE = 2.23$ ms). Further sequence parameters included: TR = 300 ms, flip angle $\alpha = 35^\circ$ (based on the previously determined T_1 relaxation time constant),

two averages and eight scan repetitions. Acquisition time was TA = 34 h 8 min.

2. A 3D multi-echo spin-echo (MESE) sequence with matrix size $280 \times 150 \times 150$, FoV = $(28 \times 15 \times 15)$ mm³, TR = 2000 ms, $\alpha_{exc} = 90^\circ$, $\alpha_{refc} = 180^\circ$, 20 equidistant echoes ($TE_1 = 4.91$ ms, $TE_{20} = 98.2$ ms, $\Delta TE = 4.91$ ms) and one single acquisition. Acquisition time was TA = 12 h 30 min.
3. A 3D variable flip angle RARE (Rapid Acquisition with Relaxation Enhancement) spin-echo sequence with matrix size $220 \times 150 \times 150$, FoV = $(22 \times 15 \times 15)$ mm³, TR = 2000 ms, $\alpha_{exc} = 90^\circ$ and variable refocusing flip angles. The sequence was optimized for tissue contrast using Bloch simulations using the previously determined tissue relaxation times $T_1 = 1450$ ms and $T_2 = 27$ ms. Acquisition time was TA = 5 h 20 min.

2.3 | Histological assessment

After the MRI scans, the tonsil was carefully removed from the PP tube, the superabsorbent was washed off with saline solution, and the specimen was prepared for histological dissection. The tonsil was again fixed with 4% formalin solution for 24 h at 4°C and embedded in paraffin. Sectioning of the tonsil was performed using a microtome (Leica). The entire tonsil was cut into 5 μ m thick slices. Hematoxylin-eosin (H&E) staining was performed for histological evaluation according to the following protocol: 2x 0 min xylene, 2x 1 min ethanol, 1 min ethanol (95%), 12 min hematoxylin solution (according to Meyer), 10 min water, 1 min eosin, 3 min ethanol each (70%, 95%, 100%), 1 min xylene and 30 min xylene. Microscope images were acquired at 20x magnification using a high-resolution slide scanner (NanoZoomer SQ, Hamamatsu).

2.4 | MRI data processing

Quantitative T_2^* maps were calculated from the MEGE-data by fitting a three-parameter exponential function in each voxel to the squared echo signals (Dietrich et al., 2001; Gudbjartsson & Patz, 1995; Henkelman, 1985):

$$S^2(TE) = S_0 \cdot e^{-2TE/T_2^*} + c \quad (1)$$

where S_0 denotes the squared nominal signal at $t = 0$ and T_2^* the fitted time constant to the signal decay. The use of the squared signal S^2 allows, as a first order approximation, the use of a fitted constant offset c to compensate for the Rician noise bias of MRI magnitude data (Gudbjartsson & Patz, 1995). Because of observed phase inconsistencies and spatial shifts in the data that occurred in the first repetition of data acquisition, this dataset was discarded. Prior to data reconstruction and analysis, data from repetitions 2 to 8 were averaged. To further reduce noise in the display of magnitude images, the images of echoes 5 through 18 were averaged, whereas the images of echoes 1 through 4 were removed due to low tissue contrast, as were the

images of the last two echoes because of the presence of substantial susceptibility artifacts.

Data acquired with the MESE sequence were analyzed in the same manner as the MEGE sequence data by using Equation (1) to calculate corresponding T_2 maps. To display magnitude images with reduced noise, images of echoes 5–20 were averaged, omitting the first four echoes because the latter did not contribute to tissue contrast.

The RARE sequence provided only single-echo images with no further processing required.

2.5 | Co-registration of MRI data to histology

Although the histological images provide an extremely high in-plane resolution, but at slice positions spaced at 50 μm , interpolation of the histological data along the latter direction may result in loss of resolution. By contrast, the isotropic acquired MRI data (with 100 μm^3 resolution) can be interpolated with almost no loss of image quality to match the histological slice orientation and position. Due to the non-negligible in-plane distortions originating from the histologic slicing process, the slice orientation adjustment was performed manually by visually matching the MRI orientation to the histology. All three MRI contrasts were then interpolated to the exact same orientation (MATLAB R2018a, The MathWorks Inc). To create a 3D model of the histologic data comparable to the three-dimensional MRI data, several pre-processing and processing steps were performed as described below.

2.6 | Image preprocessing

First, a subsample of all available histology sections was selected that contained little to no artifacts introduced by sectioning and staining the tissue. This resulted in 94 scans representing a 4.7 mm thick slab of the tonsil. The scans were manually pre-aligned with the vendor-supplied software (NDP.view2), and the original whole-slide images were exported in jpeg-format with a resolution of 3840 \times 2420 pixel. The final preprocessing steps included Gaussian smoothing and setting a manually adjusted threshold to remove non-tissue regions from the images.

2.7 | Image registration and 3D reconstruction

A pairwise image registration pipeline using SimpleElastix (Marstal et al., 2016) was implemented to align the preprocessed histology sections. The image registration pipeline consisted of three rigid registration runs followed by three affine registration runs. Here, a multi-resolution approach was applied to speed up computation and increase robustness (Borgefors, 1988). Non-affine registration steps were considered and tested, but the resulting local deformations were deemed to misrepresent the actual tissue. The registration runs were performed in an alternating fashion, using either the first or the last image as reference.

This choice of reference is less subjective than selecting a reference slice based on its appearance (Pichat et al., 2018).

To visualize the histology model created in this way and compare it with the MRI data, we used 3D Slicer, a free and open source software platform for analyzing and visualizing medical images (Fedorov et al., 2012). This allows camera movements to achieve different viewing angles as well as clipping and cropping to visualize different regions of interest.

2.8 | 3D anatomical drawing

All image data, including histology and MRI data, were given to a scientific graphic artist (Jens Geiling) and discussed with him. Based on these data and using Adobe Photoshop CC, (Adobe Systems Software), an anatomical drawing model of the tonsil was created.

3 | RESULTS AND DISCUSSION

3.1 | MRI imaging

Figure 1 shows histologic H&E-stained tonsil sections along with the corresponding matched high-resolution 9.4 T MR images, illustrating the good agreement between the two modalities. In particular, the resolution of the acquired isotropic MRI images allows clear delineation of the major anatomic structures of the tonsil, which is further supported by the information provided in the Supplementary Material. Figure S1 adds quantitative information in form of T_2^* and T_2 parameter maps, which show high similarity and allow identification of blood vessels and possible blood clots as well as lymphoid follicles based on their different quantitative T_2^* and T_2 values. Further observations included high contrast between the septum and lymphoid tissue on MEGE magnitude images (Figure S1B) as well as overall good anatomical differentiation and clear delineation of the lymphoid follicles on the spin echo-based magnitude RARE and MESE images (Figure S1D–E).

3.2 | Histology

Figure 2 shows a single high-resolution image of a tissue section from the tonsil together with annotations. The major anatomical structures are clearly visible. Based on these high-resolution sections, a 3D model was assembled using the free software tool (www.slicer.org) as shown in Figure S2 both in its entirety and with an exemplary clipping. A video of this 3D model is also available online (Video S1). Although distortions that can occur when cutting tissue sections and applying them to glass slides can occur were not considered in the standard co-registration performed, the latter was judged to be sufficiently accurate. Further refinements are to be expected when applying more complex affine co-registration tools (Lotz et al., 2017).

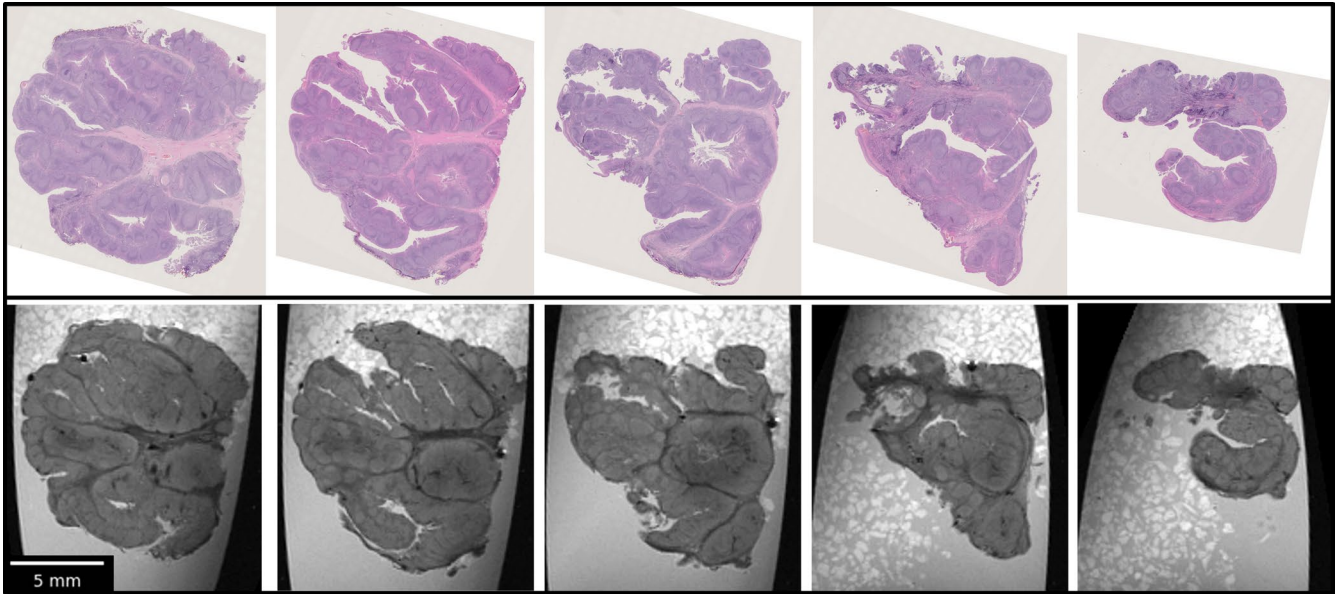


FIGURE 1 Exemplary position-matched sections are shown. Top row: H&E stained histology. Bottom row: echo averaged MESE images. MRI plane positions correspond to the histology planes at 1500, 2250, 3500, 5000 and 5800 μm (left to right). A panel with all matched sections from 0 to 6450 μm is available as a supplementary file (Figure S2)

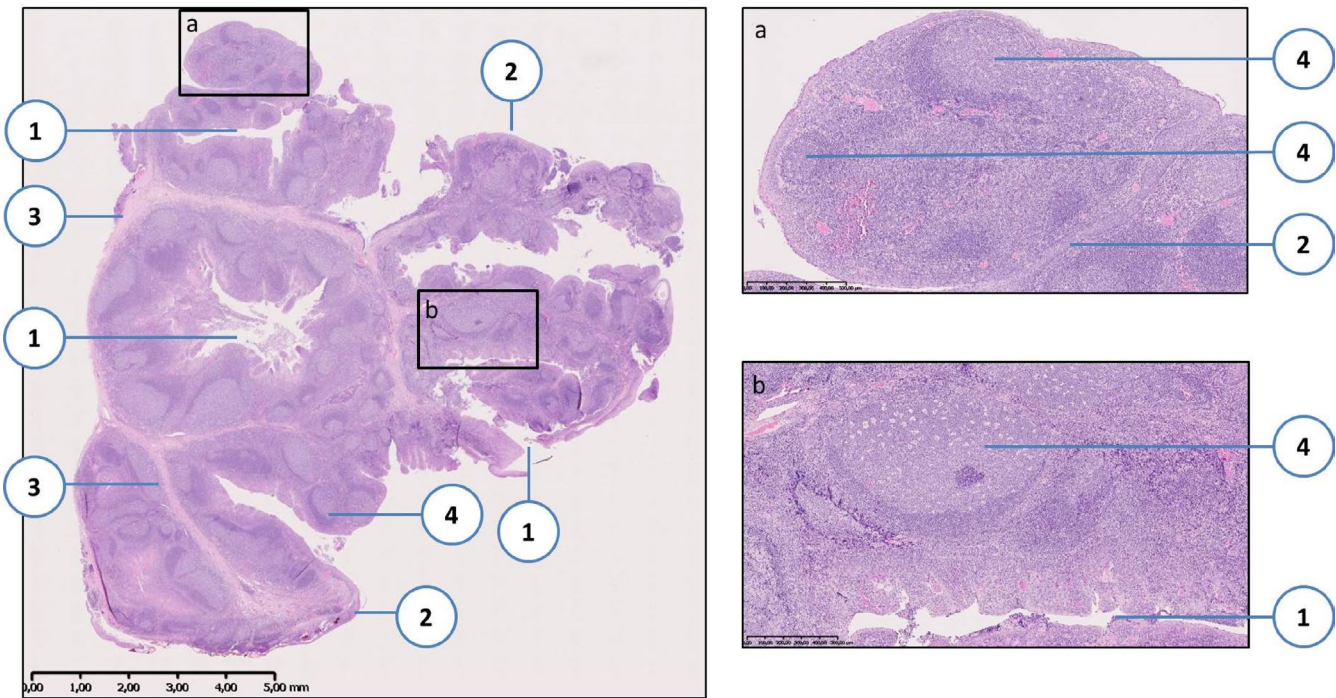


FIGURE 2 Histological image of one exemplary section. Tissue section stained according to H&E. 1: crypt, 2: epithelium, 3: connective tissue (septum), 4: lymph follicle

3.3 | Combining image data

Figure 3 shows a comparison between a stained exemplary tissue section, the corresponding MRI slice as well as the resulting 3D model. All important anatomical structures of the tonsil are clearly visible and congruent in both the H&E-stained and MRI MEGE

images. Figure S3 shows more congruent sections of H&E-stained and MRI images.

Based on these data, including the 3D model of the H&E-stained sections, a three-dimensional drawing (Figure 3, lower part) showing the outer shape of the tonsil and providing a view of its interior with anatomical structures was created by a scientific graphic artist.

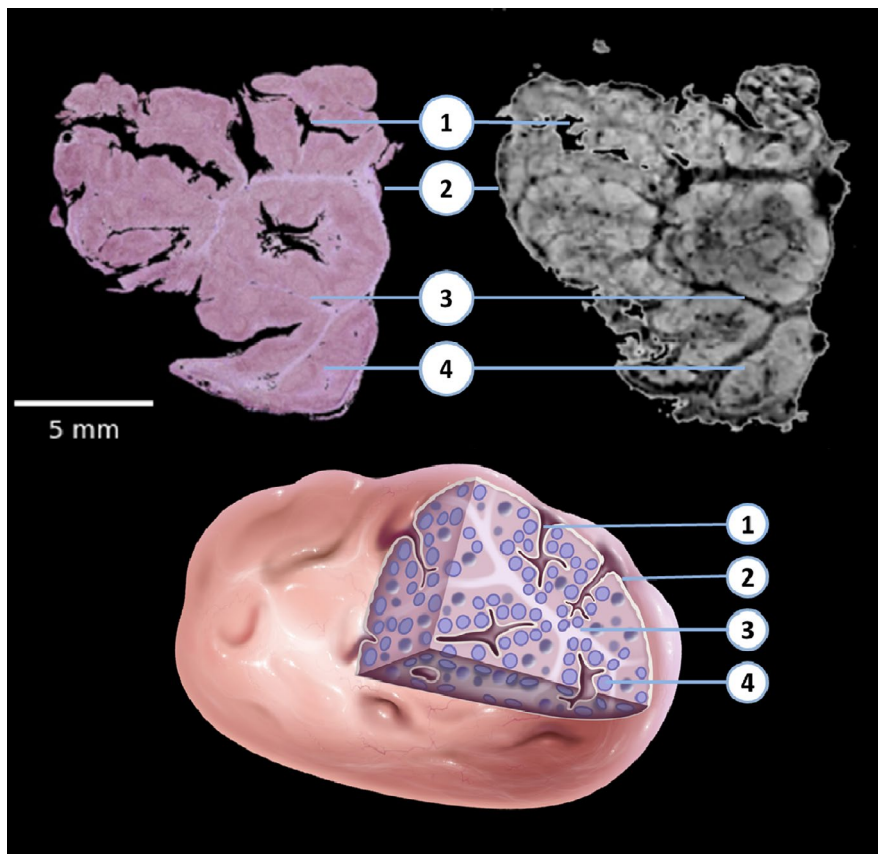


FIGURE 3 Comparison between an H&E stained tissue section image (left) with a corresponding 9.4 T MRI image slice acquired with the MEGE sequence (right) and an 3D anatomical sketch of a human tonsil based on this data (below). 1: crypt, 2: epithelium, 3: connective tissue (septum), 4: lymph follicle

4 | CONCLUSION

The aim of this study was to create compatible high-resolution imaging datasets of the same specimen using ultrahigh-field pre-clinical MRI and histological imaging techniques. Based on these data, the three-dimensional structure of the human tonsil specimen was visualized, which has not been previously presented in the literature or in anatomical textbooks.

The gold standard for exact anatomical-histological depiction of organs or parts thereof is to fix the tissue and cut it into thin tissue sections, which in turn can be assessed by staining under the microscope. While such histological sections allow visualization of structures down to the cellular level, they usually lack reference to a 3D representation of the dissected tissue sample, which is often essential for capturing the spatial extent and arrangement of anatomical structures. This modeling is further facilitated when an additional noninvasive tomographic imaging modality with high resolution, such as the MRI used here, is available that has no limitations in terms of penetration depth.

In perspective, the approach described in this study could be extended to different pathologic tonsillar conditions and their 3D anatomical representations.

DATA AVAILABILITY STATEMENT

We are not sharing our data.

ACKNOWLEDGMENTS

We thank Jens Geiling (Scientific graphic artist, Institute of Anatomy, Jena University Hospital) for designing the 3D model of a human tonsil.

AUTHOR CONTRIBUTIONS

JRR and FvE performed study concept, methodology, manuscript writing, and supervision. KHH performed data acquisition and analysis, data curation and manuscript drafting. FH performed histological project administration, methodology, validation, and manuscript writing. OGL was involved in original draft preparation and editing, data curation. KG: Tonsil surgery and preparation, DavP performed 3D registration of the H&E stained section. DanP performed Fixation, cutting and staining of the tonsil. GE (Pathologist) performed histopathological evaluation, advisor for the 3D model. All authors approved the final version.

ORCID

Ferdinand von Eggeling  <https://orcid.org/0000-0002-8062-6999>

REFERENCES

- Borgefors, G. (1988) Hierarchical chamfer matching: a parametric edge matching algorithm. *IEEE Transactions on Pattern Analysis and Machine Intelligence*, 10, 849–865.

- Dietrich, O., Heiland, S. & Sartor, K. (2001) Noise correction for the exact determination of apparent diffusion coefficients at low SNR. *Magnetic Resonance in Medicine*, 45, 448–453.
- Fedorov, A., Beichel, R., Kalpathy-Cramer, J., Finet, J., Fillion-Robin, J.-C., Pujol, S. et al. (2012) 3D Slicer as an image computing platform for the Quantitative Imaging Network. *Magnetic Resonance Imaging*, 30, 1323–1341.
- Gudbjartsson, H. & Patz, S. (1995) The rician distribution of noisy MRI data. *Magnetic Resonance in Medicine*, 34, 910–914.
- Henkelman, R.M. (1985) Measurement of signal intensities in the presence of noise in MR images: technical reports: signal intensities in MR image noise. *Medical Physics*, 12, 232–233.
- Krafft, C., von Eggeling, F., Guntinas-Lichius, O., Hartmann, A., Waldner, M.J., Neurath, M.F. et al. (2018) Perspectives, potentials and trends of ex vivo and in vivo optical molecular pathology. *Journal of Biophotonics*, 11, e201700236.
- Lotz, J.M., Hoffmann, F., Lotz, J., Heldmann, S., Trede, D., Oetjen, J. et al. (2017) Integration of 3D multimodal imaging data of a head and neck cancer and advanced feature recognition. *Biochimica et Biophysica Acta*, 1865, 946–956.
- Marstal, K., Berendsen, F., Staring, M. & Klein, S. (2016) SimpleElastix: a user-friendly, multi-lingual library for medical image registration. In: O'Conner, L. (Ed.). *2016 IEEE conference on computer vision and pattern recognition workshops (CVPRW)*. IEEE, pp. 574–582.
- Nave, H., Gebert, A. & Pabst, R. (2001) Morphology and immunology of the human palatine tonsil. *Anatomy and Embryology*, 204, 367–373.
- Pichat, J., Iglesias, J.E., Yousry, T., Ourselin, S. & Modat, M. (2018) A survey of methods for 3D histology reconstruction. *Medical Image Analysis*, 46, 73–105.
- Piqueras, S., Krafft, C., Beleites, C., Egodage, K., von Eggeling, F., Guntinas-Lichius, O. et al. (2015) Combining multiset resolution and segmentation for hyperspectral image analysis of biological tissues. *Analytica Chimica Acta*, 881, 24–36.

SUPPORTING INFORMATION

Additional supporting information may be found online in the Supporting Information section.

How to cite this article: Herrmann, K.-H., Hoffmann, F., Ernst, G., Pertzborn, D., Pelzel, D., Geißler, K., et al (2022) High-resolution MRI of the human palatine tonsil and its schematic anatomic 3D reconstruction. *Journal of Anatomy*, 240, 166–171. <https://doi.org/10.1111/joa.13532>